Journal of Robotics and Control (JRC)
Volume 5, Issue 1, 2024
ISSN: 2715-5072, DOI: 10.18196/jrc.v5i1.20302

Local-Stability Analysis of Cascaded Control for a Switching Power Converter

Mohammad Afkar [1], Roghayeh Gavagsaz-Ghoachani [2], Matheepot Phattanasak [3], Serge Pierfederici [4], Wiset Saksiri [5*]
[1, 2] Renewable Energy Department, Faculty of Mechanical and Energy Engineering, Shahid Beheshti University, Tehran, Iran
[3, 5] Department of Teacher Training in Electrical Engineering, King Mongkut's University of Technology North Bangkok, Bangkok, Thailand
[4] LEMTA, Université de Lorraine, CNRS, Nancy, France
Email: [1] en.afkar@gmail.com, [2] r_gavagsaz@sbu.ac.ir, [3] matheepot.p@fte.kmutnb.ac.th, [4] serge.pierfederici@univ-lorraine.fr, [5] wiset@kmutnb.ac.th
*Corresponding Author

***Abstract*—Switching power converters are integral in various applications like transportation and renewable energy. After their design, ensuring stable closed-loop poles is critical to maintain safe operating conditions. This study focuses on a switching DC-DC boost converter with a cascade control approach using an energy controller for the outer loop and indirect-sliding mode control for the inner loop. The research objective involves investigating stability through eigenvalue evaluation at different operating points. A large-signal average model is applied to make controlled performance independent of the operating point by fixing system poles. Nonlinear controllers, specifically indirect-sliding mode control, are chosen for their robustness, constant switching frequency, and implementation ease. Results indicate that insufficient decoupling leads to eigenvalue displacement, impacting control parameter choices. The research contribution is investigating the local stability of cascaded control, considering its advantageous implications for both performance and design. This study contributes to the understanding of switching power converters' stability, emphasizing the proposed methodology's broader applicability to diverse converter structures. The proposed approach, applicable to various switching power converters, sheds light on the importance of proper decoupling between outer and inner loop dynamics.**

Keywords—Cascaded Control; Indirect-Sliding Control; Energy; Stability; DC-DC Converters.

I. INTRODUCTION

In recent years, photovoltaic (PV) systems have played an essential role in the world, as detailed in literature. The number of publications has risen recently. To use the PV, characteristics of a photovoltaic cell must be studied. In [1], a portable photovoltaic I–V curve tracer has been proposed to study the characteristics of PV, such as performance, and identify faults or aging effects.

A. Structure of Converters

A step-up converter commonly uses a low voltage PV supplying energy to load. Different topologies have been proposed to improve both efficiency and higher-voltage step ratio. In [2], a high-step voltage ratio with multi-port cascaded DC/DC converter is proposed to serve in photovoltaic power generation systems. It presented a submodule with an isolated transformer. Using several submodules connected to PV and feeding power to a high-voltage DC bus, the output of each submodule is connected in series. In that way, the output voltage is high. In [3], a hybrid resonant ZVZCS three-level converter suitable for a photovoltaic power DC distribution system is proposed. It benefits from zero switching. Therefore, its efficiency is high. It uses a dual transformer with two output filter capacitors is proposed in this paper, which is suitable for application in distributed photovoltaic power generation at medium voltage integrated with a DC distribution network. In [4], a partial power DC-DC converter for photovoltaic systems is investigated. In contrast to other DC-DC converters, only a tiny part of the power is processed by the converter, while the significant power flows through the converter with unity efficiency. Therefore, it offers superior overall efficiency. In [5], an ultra-gain DC-DC converter is presented. It uses only one switch.

It is based on a switched capacitor–inductor network. However, the maximum efficiency is met when the duty cycle is around 0.5. Another type of high-step voltage ratio is presented in [6]. An isolated DC-DC converter is employed for a single-phase grid-tied solar photovoltaic supply system. Many high-gain step-up DC/DC converters proposed in the literature do not share common ground and have a pulsating or discontinuous input current, making the converter unsuitable for solar photovoltaic applications. Therefore, in [7], a non-pulsating input current step-up dc/dc converter with common ground structure for photovoltaic applications.

The unidirectional structure of the converter is beneficial in terms of cost and simplicity of hardware implementation of the MV circuit components, as presented in [8]. The design of the phase-shifted full bridge DC-DC (PSFB) converter is presented considering ratings of 250 kW power, 1.2 kV input, and 20 kV output. A new DC–DC converter for photovoltaic applications is proposed in [9]. Using two switches, with three windings of coupled inductor. It offers a high step-up voltage ratio, which is mainly dependent on the number of turn ratio. The proposed converters in [10] offer a simple structure with a smooth input current, a high-voltage gain, and low-voltage stress on semiconductor devices. In addition, unlike some existing ZS-based topologies in the literature, the proposed converters do not limit the power switch's duty cycle. These characteristics make the proposed converters excellent candidates to interface a low-voltage solar photovoltaic (PV) panel with a high-voltage DC bus in PV

applications. In [11], an autotransformer forward converter with type-Zeta resonant reset (AFZ) is proposed. The main characteristics of the AFZ converter are its high versatility due to its voltage step-up and step-down capability. Using an optimized autotransformer with only two windings reduces this component's complexity and power losses, the good dynamic performances, like the forward converter ones, and the low number of components, and the simplicity and high feasibility associated with using just one active switch. Besides, the autotransformer type-Zeta resonant reset achieves soft switching transitions. In [12], an interleaved high-voltage gain DC–DC converter is proposed for use with photovoltaic (PV) systems. The voltage gain is further extended by integrating two three-winding coupled inductors (CIs) with switched capacitor cells. The energy stored in the leakage inductances is absorbed through passive diode-capacitor clamp circuits. The voltage stress of the power switches is clamped to a value far lower than the output voltage, which enables designers to select switches with low-voltage ratings. Due to the interleaved structure of the proposed converter, the input current has a small ripple, leading to the PV panels' increased lifespan. A switched-photovoltaic (SPV) DC–DC converter that switches the photovoltaic (PV) cells of a series solar string periodically in parallel to balance their voltages and extract the maximum available power under mismatch conditions is proposed in [13]. Without any assistance from an external DC–DC converter, the SPV converter exploits the intrinsic capacitance of the PV cells to establish an implicit 1: n switched-capacitor (SC) converter that allows the extra current of the stronger cells in the string to flow around the underperforming cells to the output, instead of getting shunted to the ground. In [14], a multi-port modular DC–DC converter with a low-loss series LC power balancing unit (PBU) is proposed to deal with voltage imbalance due to mismatched input power. Each submodule consists of a full-bridge (FB) circuit on the PV side and a half-bridge (HB) circuit on the grid side. It contributes to the low-cost and low-loss characteristics of the converter. In [15], a current-fed dual-inductor resonant full-bridge DC–DC isolated boost converter is proposed. The converter is most suitable for applications with wide input voltage and load ranges. It removes all major drawbacks of conventional current-fed isolated DC–DC converters, such as high-voltage spikes across the switches due to transformer leakage inductance. Soft-switching rectifier diodes and clamping power switches are load-independent, leading to good efficiency over the entire load range. In [16], a novel non-isolated buck–boost dc–dc converter is introduced with a wide range of conversion ratios. Unlike the traditional one, the proposed buck–boost converter draws continuous current from its input port. Moreover, the proposed converter has a high step-up voltage gain. In [17], the authors have proposed the use of a switched converter based on the reduced redundant power processing (R2P2) concept to satisfy high current levels and low voltages in a photovoltaic system, where the input provided by the photovoltaic panels is maintained continuously.

Other types of DC-DC converters interface PV to other storage devices by extending the connectivity of ports. It forms the converters with multiple input-output ports. Depending on applications, some applications may need bidirectional power flow capability, as shown in [18]-[27]. In [18], they proposed a triple port DC-DC buck-boost converter for high step-up/step-down applications. It has two unidirectional ports and one bi-directional port for harnessing photovoltaic energy and charging the battery. The combined structure of buck and buck-boost converter is used with a particular arrangement of switches and inductors. The step-up/step-down voltage conversion ratio is higher than the conventional buck-boost converter, and the polarity of the output voltage is maintained positive. The battery is added at the bi-directional port to store energy through the bi-directional boost converter. In [19], an integrated, four-port, DC-DC converter for power management of a hybrid wind and solar energy system is proposed. Compared with existing four-port DC-DC converters, the proposed converter has the advantage of using a simple topology to interface sources of different voltage/current characteristics. Moreover, the output port is isolated using a transformer. In [20], a multi-port dc–ac converter (MPC) with differential power processing dc–dc converter (DPPC) is proposed the two ports system for battery ESS integrated PV systems. In [21], a bidirectional four-port DC–DC converter with isolation on one port is proposed. A four-port converter for PV and battery is proposed in [22] for applications where isolating ports are not required.

An integrated topology of an isolated three-port DC-DC converter (TPC) to interface Photovoltaic (PV) and battery for a stand-alone system is proposed in [23]. A boost-type three-port resonant forward converter with flexible power flow path optimization for PV systems is proposed in [24].

Nonisolated multi-port converters based on the integration of a PWM converter and phase-shift-switched capacitor converter are proposed in [25]. In [26], the authors propose novel nonisolated multi-port converters (MPCs) integrating a bidirectional pulse-width modulation (PWM) converter and a phase-shift-switched capacitor converter (PS-SCC) for stand-alone PV systems. In [26], a novel four-port nonisolated DC-DC converter for interfacing solar pv–fuel cell hybrid sources with low-voltage bipolar DC microgrids is proposed.

Distributing energy to the grid is important. A thorough study of DC-DC conversion systems for a medium-voltage DC grid-connected PV system is conducted in [27]. The two existing conversion system configurations and a proposed solution are compared regarding input/output performance, conversion efficiency, modulation method, control complexity, power density, reliability, and hardware cost. An in-depth analysis selects the most suitable conversion systems in various application scenarios.

Due to the unpredictable and fluctuating nature of solar photovoltaic (PV), energy storage systems (ESS), such as batteries, are always integrated with PV systems to smooth the power supply. In [28], a multi-port DC-AC converter (MPC) with differential power processing DC-DC converter (DPPC) is proposed for battery ESS integrated PV systems. In [29], a cascaded DC-DC converter is used to connect a medium-voltage PV system to an AC grid. Also, in [30], a

DC-DC converter connected to PV feeding an AC grid is proposed, specifically considering total harmonic distortion.

A controller to regulate inductor current and capacitor voltage should be used to use a DC-DC converter, which usually faces uncertainties such as load change or variation on input voltage. There are several control methods in literature proposed to control such a system. In [31], parametric independent control of the DC-DC boost converter using a two-degree-of-freedom internal model control scheme has been proposed. This control is based on linear control theory. Most of the works reported in the literature for control and stability analysis of these configurations are based on small-signal AC models. This could be a significant limitation, as this kind of linearization produces a good approximation of the nonlinear model of series-connected dc/dc converters only at the operating point. However, PV systems must be controlled for large operating points with satisfactory performance and robustness. The control scheme can handle the set point and the load-disturbance response separately. In contrast, in [32], the authors proposed to use a nonlinear control dealing with internal stability for a series of boost converters in a PV system. In [33], the authors present an Internet of Things (IoT) solution for controlling and monitoring a low-power photovoltaic system (250 W). Power conditioning is performed by a DC-DC Flyback converter with active clamping. An ESP32 microcontroller is used to implement an output voltage control loop and to communicate, online and in real-time, with an internet server. In [34], two storage devices are used in a system with a PV connecting to a load. An improved virtual capacitor (IVC) parallel coordination control strategy is proposed based on a multi-port isolated DC-DC converter. The MPIC is used to replace the traditional Buck/Boost circuit to achieve electrical isolation from the micro sources of the energy storage system. The authors present a methodology to control the internal energy balance of a modular multilevel cascade converter (MMCC) with distributed energy resources [35]. The converter is characterized by a high-voltage multi-terminal DC link connected to a three-phase MMCC with distributed photovoltaic arrays, including wind turbines.

B. Significant of Maximum Power Point Tracking

A maximum power point tracking (MPPT) algorithm must be performed to use PV and ensure that the maximum power is acquired. Several articles are dedicated to this topic. In [36], the authors proposed 1-new high step-up DC/DC converter 2-model predictive control based maximum power point tracking (MPC-MPPT) algorithm with an optimum number of sensors. In [37], a global maximum power point tracking (GMPPT) is presented. It is a review article demonstrating that DC-DC converters with a wide input voltage range can enable GMPPT to gain higher efficiency than others. As partial shading is one of the most common problems for PV, a deterministic particle swarm optimization to improve the maximum power point tracking (MPPT) capability for photovoltaic systems is presented in [38]. Also, in [39], a fuzzy logic control-based maximum power point tracking technique in a stand-alone photovoltaic system is presented using simulation. It is further implemented and experimented in [40]. The MPPT can also be used at a trim power level in an on-chip PV [41]. MPPT is still a very active domain; in [42], an improved P & O MPPT was improved and called IP & O. The efficiency of the proposed converter was estimated to be over 95% at various power levels. In a classic MPPT, several sensors should be used. It is costly. In [43], a current sensorless delay-based controller is proposed for the closed-loop stabilization of a photovoltaic system under an MPPT scheme using a boost dc/dc converter. It used only two voltage sensors. To further improve the performance of the conventional perturb and observe (P&O) maximum power point tracking (MPPT) algorithm where the oscillation around the maximum power point (MPP) is the main disadvantage of this technique, the article [44] introduces a modified P&O algorithm to conquer this handicap. The new algorithm recognizes approaching the peak of the photovoltaic (PV) array power curve and prevents the oscillation around the MPP. In [45], the novel algorithm for optimal sizing of stand-alone photovoltaic pumping systems is presented. It presented a way to choose the right size of PV systems.

The performance of PV modules is investigated in different aspects: partial shading [46]-[50], degradation [51]-[52].

Apart from the studies of MPPT with the proposed converter mentioned before, the MPPT algorithms are proposed in [53]- [54]. The new maximum power point tracking approach using a genetic algorithm is presented in [53] and uses a particle swarm optimization (MPSO) [54].

The connection of PV is also essential. Series and parallel connections depend on the design of such applications [55]. Using a bypass diode is very important to protect the PV panel and reduce the shading effect to improve the overall efficiency [56].

C. Significant of Controllers

Using MPPT, two interesting approaches are controlling the PV current, and energy stored in a parallel capacitor PV. To do that, the MPPT provides a reference signal to the controller to ensure that the control objective is achieved in a finite time. The sliding mode controller, which is a nonlinear controller, is investigated for a quadratic boost converter [57]. It is also applied to a classic boost converter [58] and a complicated Z-source inverter [59]. With the evidence in [57]-[58], it is recommended to use the sliding mode controller for MPPT.

These circumstances can cause panels' electricity production mismatches, notably in urban contexts. For the series PV modules, in mismatching cases, the bypass diode can be activated for the lower insolated modules where there is a voltage difference for other modules. Therefore, the PV characteristic has at least two peaks for several series strings. The maximum power point tracking (MPPT) algorithm has difficulty finding the absolute maximum point from the local maximum. As a result, in this situation where the operating point for photovoltaic systems changes, it is vital to choose a suitable controller.

When the current controller is independent of the equilibrium point, the dynamic performance of the controlled system remains the same even if its operating point changes.

For example, in a PV system, when the temperature change or partial shading occurs, the operating point of the system changes, but the dynamic performance of the controlled system remains the same. This can easily design the window of MPPT compared to the controller, which depends on the operating point.

A nonlinear controller such as sliding-mode control has been used for its high dynamic performance and outstanding robustness concerning external disturbances, uncertainties, or parameter variations. Within various categories of nonlinear controllers, sliding-mode control employing an indirect approach presents the primary benefit of maintaining a constant switching frequency. The control parameters align precisely with the selected pole locations, simplifying the task for the designer in setting and adjusting these control parameters.

Using MPPT, an interesting approach is controlling the PV current of PV. To do that, the MPPT provides a reference signal to the controller to ensure that the control objective is achieved in a finite time. The sliding mode controller is investigated for a quadratic boost converter [57]. It is also applied to a classic boost converter [58] and a complicated Z-source inverter [59]. With the evidence in [57]-[58], it is recommended to use the sliding mode controller for MPPT.

This paper uses two controllers, the control of inductor current and energy stored in a capacitor with dynamical properties autonomous of the operating conditions. An indirect sliding mode controller is utilized instead of a conventional one.

The term depending on the sign of the system trajectory, can be used to converge on the surface when the trajectory is far from the surface [58]. Furthermore, in this work, the term for the error is omitted, which prevents the chattering problem. In fact, in the indirect synthesis, the state of the system is increased by the integral component. This integral term allows for ensuring zero static error. Therefore, these advantages can be summarized as follows:

- fixed switching frequency,
- no steady-state error,
- no chattering effect.

In some complicated structures of converters, energy control is suggested instead of voltage control. In this paper, the outer loop of the control system is responsible for regulating the energy stored in the output capacitor. It has been specifically chosen due to its superior dynamic behavior compared to the voltage controller, mainly when constant power loads are employed [59].

In the literature, several articles propose the control in a cascaded manner by using a rule of thumps that the poles of the controlled loop must be separated at least 10 times [58]-[59]. Typically, designers resort to employing a Bode diagram to configure control parameters, assuming effective decoupling of the inner and outer loops and treating the inner loop as a gain. However, it is rare to study the actual poles that have been placed using such a rule. Therefore, in this paper, we proposed to fill the gap by investigating the locations of actual poles concerning the placing poles.

The research contribution lies in examining the local stability of cascaded control utilizing indirect-sliding mode and energy concepts, owing to their advantageous implications for performance and design. This investigation is distinct in establishing closed-loop poles independently of operating points by employing nonlinear controllers based on a large-signal averaged model, eliminating the need for small-signal linearization. The study also delves into the comprehensive separation dynamics of both the inner and outer loops.

The organization of this paper is as follows. Section 2 presents the method for this study, including the power stage, controllers, and modeling for obtaining the eigenvalues. Section 3 presents the results and discussion. Finally, the conclusions are drawn in Section 4.

II. METHOD

In this section, the studied system, including the boost converter with its controllers, is presented. In the first step, in Section 2.1, the power stage will be given. In the second step, in Section 2.2, the two controllers will be presented. Finally, the model of the studied system will be given in Section 2B

A. Power Stage

The DC-DC boost converter (Fig. 1) [60]. The passive elements are inductor with series resistance (L, r_L), and capacitor (C). The system fed by the input voltage source (V_i) such as PV system. The load current is $i_{out} = \frac{v_C}{R}$ where R is load resistance. The switch K, diode D, and capacitor C are assumed to be ideal. The converter is operated by controlling the switch K to be on or off with a constant switching frequency F_s relating to a switching period $T = \frac{1}{F_s}$. The switching command u linked to d where d represents the duty cycle defined as the ratio of the duration of the turn-on (T_{on}) to the switching frequency (T):

$$\boldsymbol{d = T_{on}/T} \tag{1}$$

The converter is functioning in continuous conduction mode (CCM), which means that the inductor current is always higher than zero.

The state equation of the DC-DC boost converter can be put into the form:

$$\begin{cases} \frac{di_L}{dt} = \frac{1}{L}(\boldsymbol{V_i - r_L \cdot i_L - (1-d)v_C}) \\ \frac{dv_C}{dt} = \frac{1}{C}\big((\boldsymbol{1-d})\boldsymbol{i_L - i_{out}}\big) \end{cases} \tag{2}$$

where $\boldsymbol{x = [i_L\ v_C]^T}$ is the state vector comprising inductive currents and output capacitor voltage.

B. Controllers

In this part, two controllers are presented for the boost converter. The block diagram of the cascaded control scheme is given in Fig. 1, which will be detailed in this section.

The controllers are designed to maintain predetermined values for the inductor current and output capacitor voltage, defining a safety operation zone crucial for overall system

protection. Prioritizing the slow dynamics of the output capacitor voltage, the cascaded control scheme is initiated. Subsequently, the controller identifies errors stemming from both transient and steady-state conditions, generating an appropriate current reference. This reference is then utilized to regulate the current drawn from the source through the inductor. The slower outer control loop focuses on the output voltage, while the faster inner control loop addresses the inductor current.

The control of the studied system is implemented using nonlinear controllers. The converter command is founded on inner and outer loops, as presented in Fig. 2.

The energy y in the output capacitor C is controlled by the outer loop control. This energy controller is selected since the dynamic behavior is better than the voltage controller, as mentioned earlier. The current reference is generated by the energy controller. The inductive current is controlled by the inner loop. The command of the switch u is generated with a symmetric pulse-width modulator (PWM), as shown in Fig. 3. In the following, the details of the controllers will be presented.

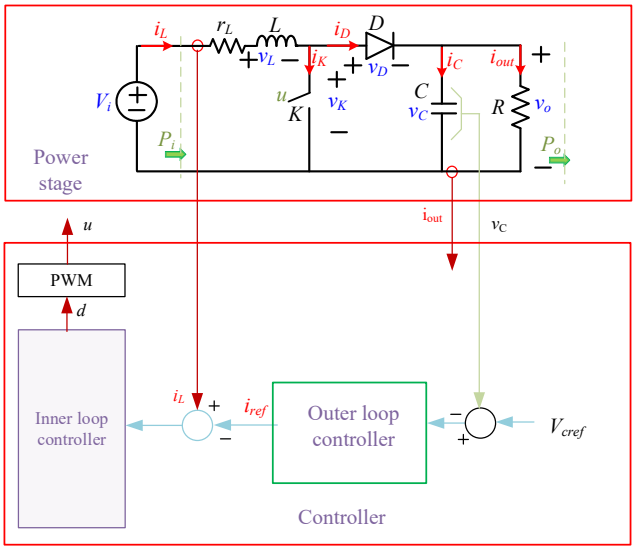

Fig. 1. Illustration of the studied system with cascaded control

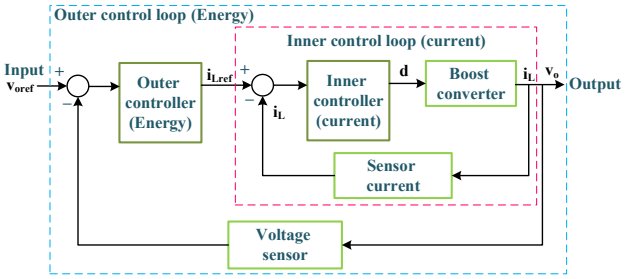

Fig. 2. Cascaded control structure consists of inner-current loop and outer energy loop

1) Outer Control Loop

To control the output voltage, the energy stored in the capacitor is considered instead of the output voltage. Because its dynamics depends directly on the associated powers, which are easy to deal with. The energy stored in the output capacitor is given by:

$$y = \frac{1}{2} C v_C^2 \tag{3}$$

where v_c is the output capacitor voltage.

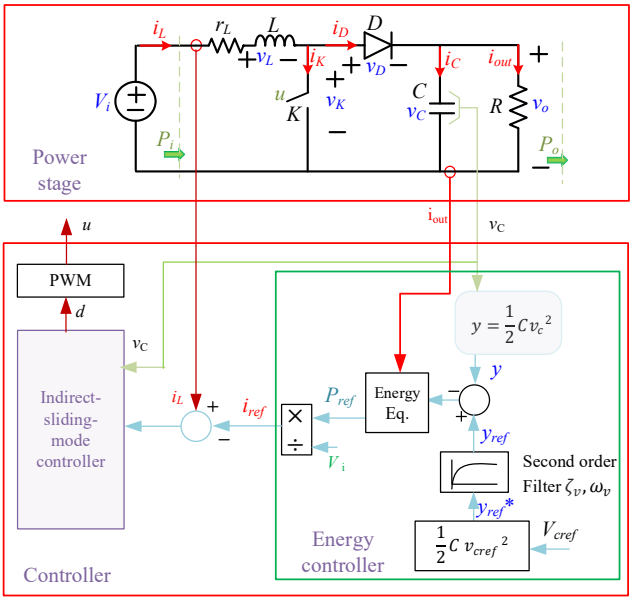

Fig. 3. Control block diagram linked to the converter

The energy reference is $y_{ref}^* = 0.5\ C\ V_{Cref}^2$ where V_{Cref} is the output voltage reference. To limit the capacitor current in startup regime, the second-order filter, with a unity damping factor and cutoff frequency ω_v, is used to make the energy reference change smoothly from the initial condition to the value of y_{ref}.

The energy controller is defined by the following equation [60], [61]:

$$\frac{dy}{dt} - \frac{dy_{ref}}{dt} + K_{py}(y - y_{ref}) + K_{iy}\int(y - y_{ref})dt = 0 \tag{4}$$

where $\frac{dy}{dt}$ is the derivative of y. The system response conforms to a second-order structure [62]-[63] expressed as:

$$s^2 + 2\zeta\omega_n s + \omega_n^2 = 0 \tag{5}$$

The coefficients can be selectively determined to guarantee the stability of the system [64]. Therefore, the coefficients of the controller can be defined as:

$$K_{py} = 2\zeta\omega_n \tag{6}$$

$$K_{iy} = {\omega_n}^2 \tag{7}$$

where ζ is the damping factor, and ω_n is the cutoff angular frequency corresponding to the control bandwidth of the controlled system [65]-[66]. Thanks to the energy controller, the current reference i_{ref} can be obtained. It can be done using the input-output power balance relation [67]-[68]:

$$\frac{dy}{dt} = P_i - P_o \rightarrow \frac{dy}{dt} = V_i\, i_L - r_L\, i_L^2 - v_C i_{out} \tag{8}$$

where $i_{out} = \frac{v_C}{R}$.

Using (4), the second-order equation in (8) can be solved. Since the output voltage reference is constant in steady state, therefore, in (4) $\frac{dy_{ref}}{dt} = 0$. The current reference i_{ref} is obtained as (9).

$$\boldsymbol{i_{ref}} = \frac{\boldsymbol{2P_{max}}}{\boldsymbol{V_i}}\left[\boldsymbol{1} - \sqrt{\boldsymbol{1} - \frac{\boldsymbol{P_p}}{\boldsymbol{P_{max}}}}\ \right] \quad (9)$$

where $P_p = v_C\, i_{out} - K_{py}(y - y_{ref}) - K_{iy}\int(y - y_{ref})dt$, and $P_{max} \triangleq \frac{{V_i}^2}{4r_L}$ [69]-[70].

The current reference i_{ref} is the input of the inner current loop. This loop will be detailed in the following subsection.

2) Inner Control Loop

The inner loop is based on an indirect-sliding mode controller. This controller uses the following sliding surface S [71]-[73]:

$$\boldsymbol{S = i_L - i_{ref} + K_i\ \int(i_L - i_{ref})dt} \quad (10)$$

The equation (11) is executed on the derivative of S [62]:

$$\frac{\boldsymbol{dS}}{\boldsymbol{dt}} = \boldsymbol{-\lambda S} \quad (11)$$

Since the current reference i_{ref} is not constant. Therefore, its derivative is not zero. In the following, the calculation of this term is presented. The current reference in (9) is in the function of the output capacitor voltage v_C and integral term of the energy $inty = \int(y - y_{ref})dt$. Therefore, the derivative of the current reference can be calculated using (12).

$$\frac{\boldsymbol{di_{ref}}}{\boldsymbol{dt}} = \frac{\boldsymbol{di_{ref}}}{\boldsymbol{dv_C}}\frac{\boldsymbol{dv_C}}{\boldsymbol{dt}} + \frac{\boldsymbol{di_{ref}}}{\boldsymbol{dinty}}\frac{\boldsymbol{dinty}}{\boldsymbol{dt}} \quad (12)$$

where $\frac{dv_C}{dt}$ is already defined in (2) and $\frac{dinty}{dt} = y - y_{ref}$.

Using the differential equation of the inductor current in (2) and (10)-(11), and (12), the duty cycle d is calculated as (13).

$$\boldsymbol{d = f(i_L, v_C, \int(i_L - i_{ref})dt, \int(y - y_{ref})dt)} \quad (13)$$

C. Modeling

In the first step, the model will be given in Section 1). In the second step, in Subsection 2), the operating point calculation will be presented. To calculate the eigenvalues, the operating point (equilibrium point) of all variables is necessary [74]-[75].

1) Model

Using the equations to describe the behavior of the studied converter and the controllers presented in the previous section, a vector $X \in \mathbb{R}^4$ can be defined as follows:

$$[\boldsymbol{X}] = \begin{bmatrix}\boldsymbol{X_1}\\ \boldsymbol{X_2}\\ \boldsymbol{X_3}\\ \boldsymbol{X_4}\end{bmatrix} = \begin{bmatrix}\boldsymbol{\bar{i}_L}\\ \boldsymbol{\bar{v}_C}\\ \boldsymbol{\int(\bar{i}_L - \bar{i}_{ref})dt}\\ \boldsymbol{\int(\bar{y} - \bar{y}_{ref})dt}\end{bmatrix} \quad (14)$$

where the symbol $\bar{z}$ represents the average value of the variable z calculated over one switching period [76].

As presented in (14), this average model considers system state variables (X_1 and X_2), and the controller variables (integral components X_3 and X_4). Using the system equations and duty cycle, the state vector X verifies the equation $\dot{X}$ given in (15) and (16).

$$\boldsymbol{\dot{X} = H(X)} \quad (15)$$

$$[\boldsymbol{\dot{X}}] = \begin{bmatrix}\frac{\boldsymbol{-r_L X_1 + V_i - (1-d)X_2}}{\boldsymbol{L}}\\ \frac{\boldsymbol{X_1(1-d) - i_{out}}}{\boldsymbol{C}}\\ \boldsymbol{X_1 - i_{ref}}\\ \boldsymbol{\frac{1}{2}CX_2^2 - \frac{1}{2}CV_{Cref}^2}\end{bmatrix} \quad (16)$$

The stability of the small-signal model around the operating point can be studied using the eigenvalues of matrix $H(X_0)$ [77]-[78].

2) Equilibrium Point

The equilibrium point holds significance in this context, particularly in determining the eigenvalues of the system for assessing local stability [79]-[80]. Defining the equilibrium point corresponding to each case is imperative, as the calculation of eigenvalues is contingent upon these specific equilibrium conditions.

a) Energy Stored in the Capacitor

The equilibrium capacitor energy y_0 can be defined as:

$$\boldsymbol{y_0 = \frac{1}{2}Cv_{C0}^2} \quad (17)$$

where $v_{C0} = v_{Cref}$ is the equilibrium capacitor voltage.

b) Inductor current

The equilibrium inductor current i_{L0} can be found as follows. The equilibrium current is set by the current reference i_{ref} using (7). Thus:

$$\boldsymbol{i_{L0} = i_{ref} = \frac{2P_{max}}{V_i}\left[1 - \sqrt{1 - \frac{P_p}{P_{max}}}\ \right]} \quad (18)$$

Where $P_p = v_{C0}\, i_{out} - K_{py}\frac{1}{2}C\left(v_{C0}^2 - v_{Cref}^2\right) - K_{iy}\frac{1}{2}C\int\left(v_{C0}^2 - v_{Cref}^2\right)dt$, and $P_{max} \triangleq \frac{{V_i}^2}{4r_L}$.

c) Integral Terms

The integral terms $\int(i_L - i_{Lref})dt$ and $\int(y - y_{ref})dt$ nearby the equilibrium points are zero.

In summary, the research methodology, as illustrated in Fig. 4, encompasses a series of ordered steps. The system under investigation comprises a converter and its associated control section. Derivation of the governing differential equations for the boost converter involves the application of Kirchhoff's voltage and current laws. These laws are formulated for two states, determined by the open or closed status of the switch, contingent upon the converter's circuit configuration. The control signal, influenced by the control section, dictates the switch state and the duty cycle is computed accordingly.

The proposed cascade controller comprises an outer loop responsible for capacitor energy control, effectively regulating the output voltage. Simultaneously, the inner loop manages current control, governing the input current. The energy control loop exhibits slower dynamics compared to the power control loop, a crucial consideration in determining the bandwidth of each loop for design purposes. The mathematical equations for each loop and the control block

diagram are introduced. At the control section's input, the outer loop receives the reference output voltage, generating the reference input power. This input is divided by the input voltage and then directed to the inner loop, with its output being the duty cycle. Utilizing pulse-width modulation (PWM), the duty cycle (d) is transformed into a control signal (u), and subsequently applied to the converter. The system's mathematical equations facilitate simulation, allowing for waveform analysis. The ensuing section will present the results derived from the simulation.

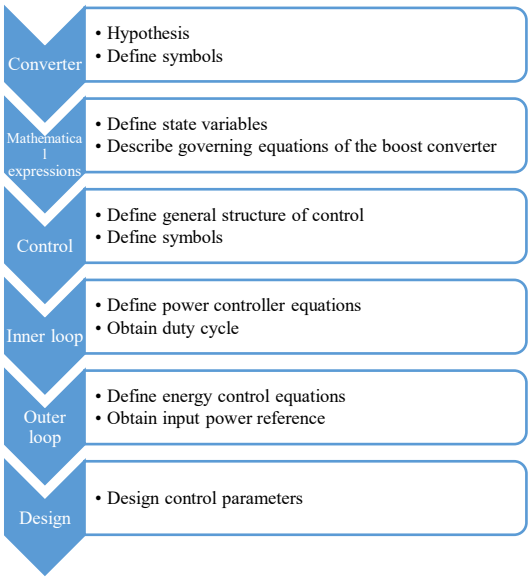

Fig. 4. Research methodology flowchart

III. RESULTS AND DISCUSSION

In this section, the results are given to validate the proposed model. The MATLAB/Simulink software is used. The used parameters are given in Table I. In Section A), the eigenvalues of the system are investigated. The two scenarios (Case 1 and Case 2) detailed in Table II are realized. The theoretical eigenvalues are also given in Table II. They are linked to control parameters. In both cases, for the inner controller, the parameters $\lambda = K_i$ is set. As mentioned above, to separate the two control loop dynamics, the eigenvalues' location of both loops must be far from each other. In Section B), the behavior of the system is presented through electrical waveforms.

TABLE I. SYSTEM PARAMETERS

Parameters	Quantity	Value
V_i	Input voltage	60 V
L	Inductance	1 mH
r_L	Inductor resistance	0.3 Ω
C	Output capacitance	1100 µF
F_s	Switching frequency	10 kHz
R	Load resistance	37.5 Ω
V_{Cref}	Voltage reference	150 V
λ	Current control parameter	3141 rad/s
K_i	Current control parameter	3141 rad/s
ω_n	Energy control parameter	See Table 2
ξ	Energy control parameter	0.707
ω_v	Second-order filter parameter	200 rad/s
ξ_v	Second-order filter parameter	1

TABLE II. TWO SCENARIOS

Case	Loop	Nature of Eigenvalues		Remark	Theoretical eigenvalues
		Real	Complex		
1	Inner	*		$\lambda = K_i$	$-\lambda$
	Outer		*	$\omega_n = \frac{\lambda}{5}$ rad/s	$\omega_d = -\xi\omega_n \pm j\omega_n\sqrt{1-\xi^2}$
2	Inner	*		$\lambda = K_i$	$-\lambda$
	Outer		*	$\omega_n = \frac{\lambda}{100}$ rad/s	$\omega_d = -\xi\omega_n \pm j\omega_n\sqrt{1-\xi^2}$

A. Eigenvalues

The eigenvalues of the system matrix, also known as the state transition matrix, within the state space correspond to the poles of the system transfer function. Consequently, these eigenvalues serve as predictive indicators of the system's stability. In the case of a stable continuous system, it is expected that the eigenvalue, or pole, resides on the left-hand side (LHS) of the imaginary axis in the s-plane.

Inappropriate and appropriate values are selected for Cases 1 and 2, respectively. In Case 1, both groups of eigenvalues' locations (for inner loop and outer loop) are lower than 1 decade. In contrast, for Case 2, both eigenvalues' location is greater than 1 decade. In other words, in Case 1, $\omega_n = \lambda/5$ rad/s and Case 2, $\omega_n = \lambda/100$ rad/s are selected.

1) Case 1

According to the model, the Jacobian matrix is a function of the operating point, then the eigenvalues of system depend on the equilibrium point. In Fig. 5, the eigenvalues of the controlled system are depicted, encompassing a set of four poles. The values of the parameters that dictate the inner control loop position the two real poles on the extreme left, where their λ value is equivalent to K_i. Furthermore, the remaining two poles appear as complex and are situated near the origin, a position determined by the outer control loop. As can be observed in Fig. 5(a), for the inappropriate choice (Case 1), before changing the operating point, the values of the obtained eigenvalues corresponding to the energy loop are negative (for $V_{cref} = V_{crefN}$). But in in Fig. 5(b), for $V_{cref} = 1.5\,V_{crefN}$, the values of the obtained eigenvalues corresponding to the energy loop are positive. Therefore, the system is unstable [78].

2) Case 2

On the other hand, for the appropriate choice (Case 2) in Fig. 6, when the eigenvalues of both control loops are decoupled ($\omega_n = \lambda/100$ rad/s), the values of the obtained eigenvalues corresponding to the energy loop are negative before and after changing the operating point (V_{cref} from V_{crefN} to $1.5\,V_{crefN}$), as expected. The eigenvalues for the inner loop are real. The eigenvalues for the outer loop are complex [79]-[80] as:

$$\boldsymbol{\omega_d = -\xi\omega_n \pm j\omega_n\sqrt{1-\xi^2}} \quad (19)$$

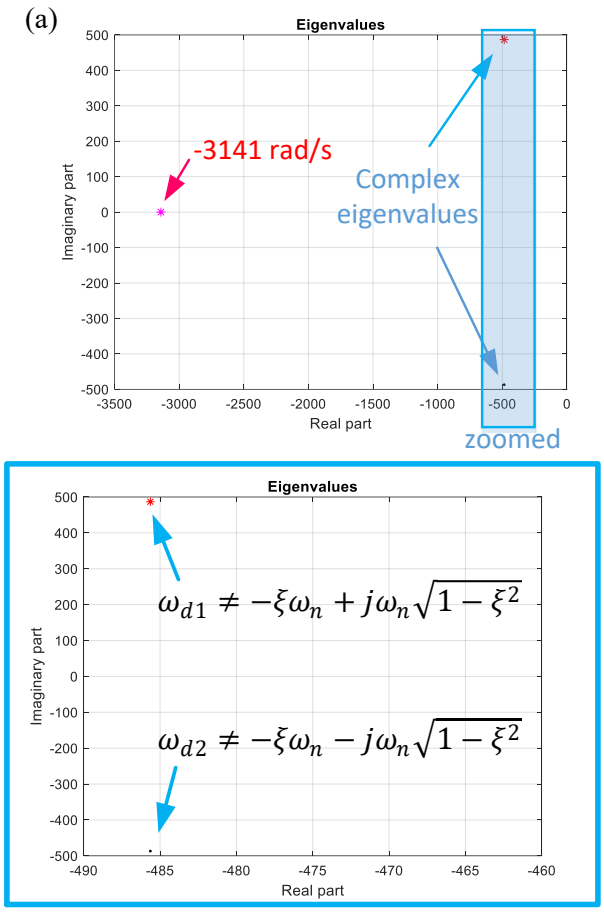

Fig. 5. Eigenvalues of the studied system (Case 1), (a): stable (b): instable system

B. Waveform

The energy reference is derived from the voltage reference and then passed through a second-order system to achieve a smooth transition from the initial point to the final point. As mentioned earlier, this approach ensures a seamless progression and minimizes any abrupt changes during the transition process.

Fig. 7 and Fig. 8 show the waveforms of the system while the output voltage reference varies from 150 V to 225 V at t = 0.05 s for Case 1 and Case 2, respectively.

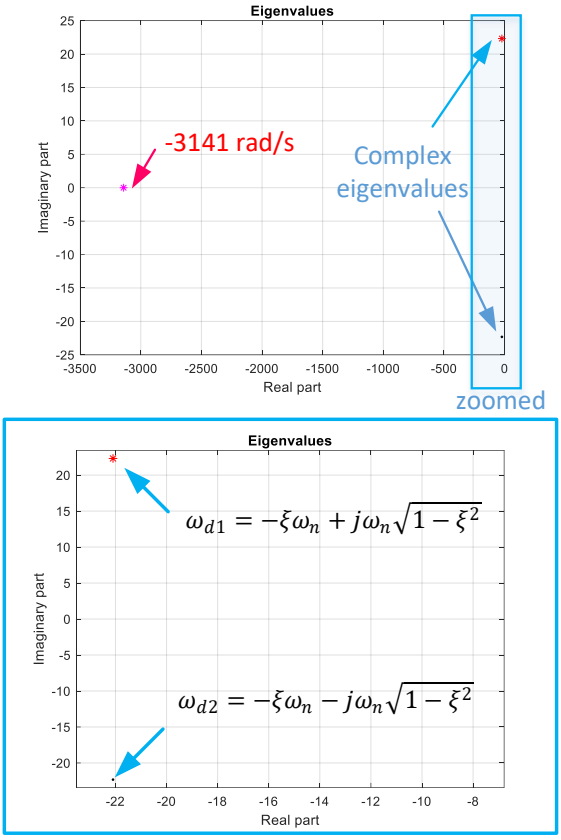

Fig. 6. Eigenvalues of the studied system (Case 2)

1) Case 1

In Case 1, the two control loop dynamics do not decouple well. Therefore, the system is unstable for changing the operating point when the output voltage reference varies from 150 V to 225 V at t = 0.05 s. Fig. 7 shows the waveforms of the system while the output voltage reference varies from 150 V to 225 V at t = 0.05 s. It is evident that the operational state of the system has undergone a modification. The alteration involves a shift in the output capacitor voltage reference, transitioning from 150 V to 225 V. To achieve the desired final value of the output capacitor voltage, an elevation in the inductor current is necessary. However, it is apparent that the inductor current, influenced by the outer loop controller, deviates from its reference. Consequently, this deviation leads to a decline in the output voltage, ultimately reaching zero.

2) Case 2

On the other hand, in Case 2, the control dynamics are well decoupled, and the system remains stable when the operating point is changed. However, the response time of the energy loop is longer than that in Case 1. It is due to small values of eigenvalues corresponding to the energy control loop. Fig. 8 shows the waveforms of the system while the output voltage reference varies from 150 V to 225 V at t = 0.05 s.

In Case 2, the control dynamics are well decoupled, and the system remains stable when the operating point is changed. However, the response time of the energy loop is

longer than that in Case 1. It is due to small values of eigenvalues corresponding to the energy control loop.

One can assume a damping factor ξ=0.707 and conducts simulations of the system using the averaged model for expeditious results. The outcomes are illustrated in Table III. It is noteworthy that smaller values of ω_{ny} lead to increased response times, as stipulated in equation (9).

TABLE III. SETLING TIME FOR DIFFERENT w_{ny}

$\omega_{ny}\ (rad/s)$	Settling time, $T_s\ (ms)$
31.41	300.5
26.17	373.2
24.16	404.3

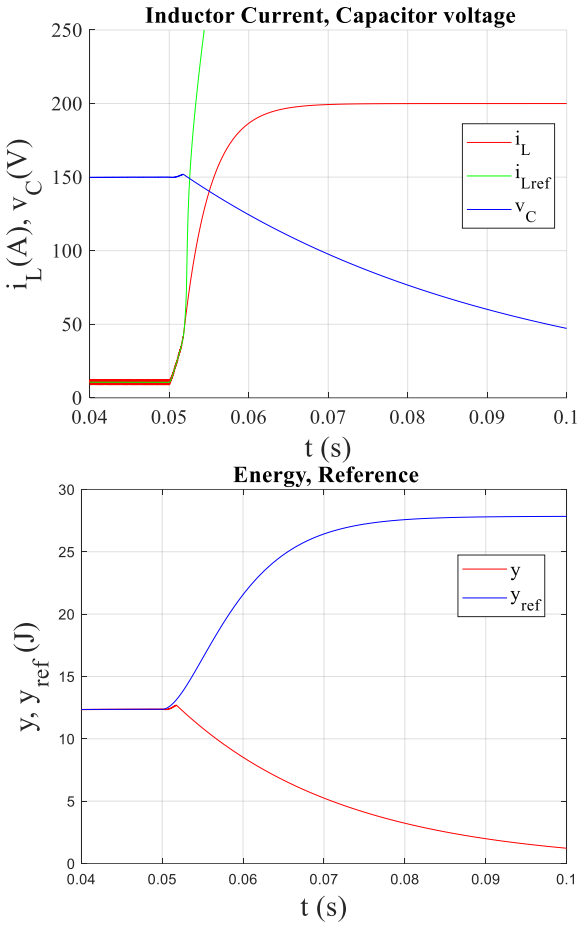

Fig. 7. Inductor current (i_L), its reference (i_{ref}), and output voltage capacitor (v_C) waveforms. Energy stored in the capacitor (y) and its reference (y_{ref}) (Case 1)

3) *Comparison to PI controller*

A comparison to a similar method from previous works [65] to enhance research contributions is provided in this section. The previous work is redesigned using the same bandwidth of both controller loops. In this test, the load step from $R = 75\ \Omega$ to $R = 37.5\ \Omega$ is applied at t = 1 s. The waveforms of the output voltage and its reference for the proposed and the PI control are given in Fig. 9. It can be seen that the response of the system with the proposed method using the indirect-sliding mode control and energy control offers a lower undershoot voltage. The waveforms of the proposed method are zoomed and given clearly in Fig. 10.

As the boost converter finds applications across diverse contexts, the operational state of the system undergoes fluctuations over time. These variations can arise from shifts in load power or alterations in the properties of parasitic elements, causing deviations from their nominal values. Such changes in stability characteristics can impact the practical deployment of the boost converter. To guarantee a consistent and reliable power supply to the load, it is crucial to maintain stable operation of the converter. Conducting a stability analysis becomes imperative to anticipate and understand the system's stability under different conditions.

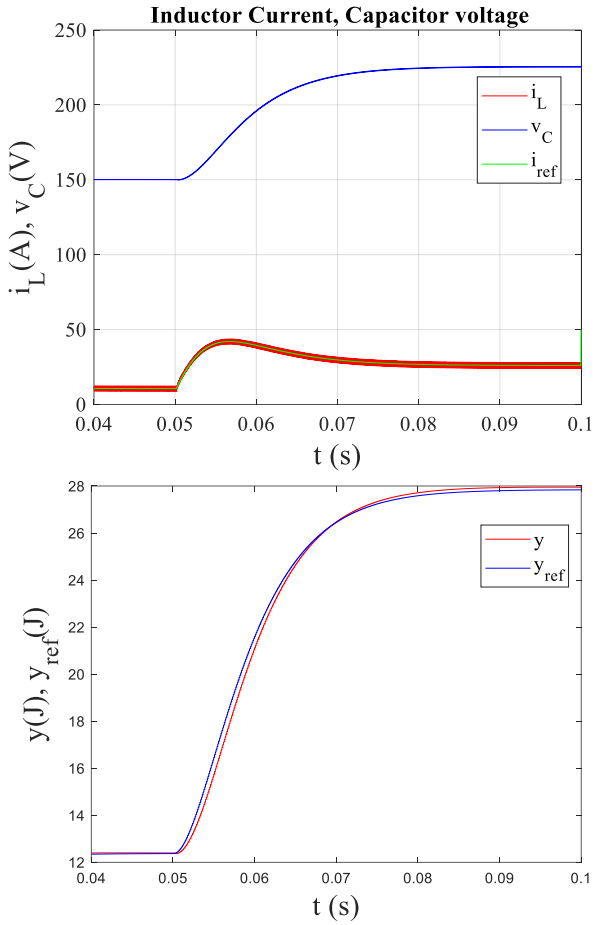

Fig. 8. Inductor current (i_L), its reference (i_{ref}), and output voltage capacitor (v_C) waveforms. Energy stored in the capacitor (y) and its reference (y_{ref}) (Case 2)

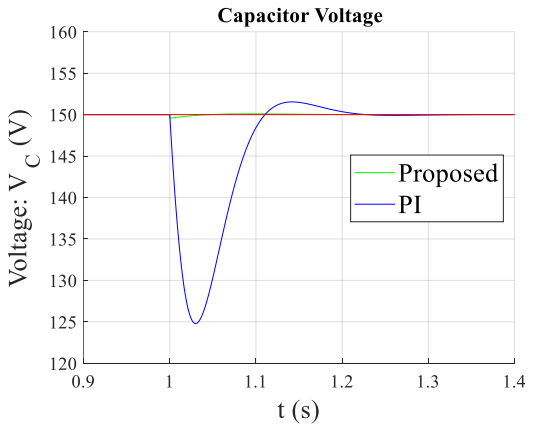

Fig. 9. Comparison of output voltage capacitor (v_C) waveforms and its reference for the proposed method and the classic PI controllers

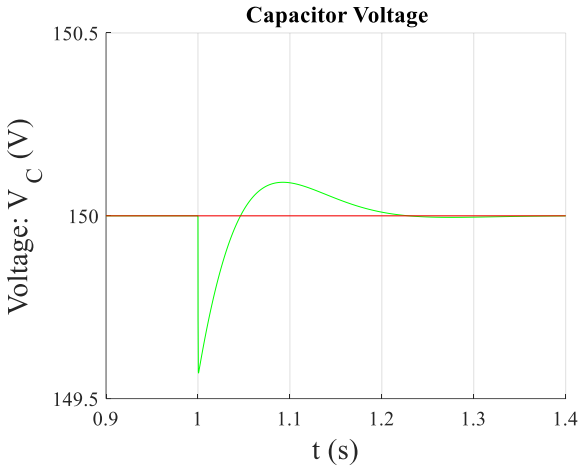

Fig. 10. Output voltage capacitor (v_c) waveforms and its reference for the proposed method

4) Strenghts and limitation

It can be performed using the controller whose designing process does not depend on the equilibrium point of the converter such as indirect-sliding mode control. It offers many advantages, for instance, robustness against uncertainty parameters, constant switching frequency, and ease of implementation.

However, when the system is well decoupled, as the eigenvalue becomes smaller than in the latter case, the response time of the energy loop becomes longer.

The limitations of this study can be outlined as follows:

i) To attain a swift response in the outer loop, there is a need to accelerate the inner loop, resulting in a subsequent demand for a higher switching frequency.

ii) The utilization of an indirect-sliding mode and energy controller entails the requirement for four sensors—specifically, two current sensors and two voltage sensors.

IV. CONCLUSION

This paper gives the design of a cascaded control scheme based on nonlinear controllers. The energy controller and indirect-sliding mode approaches are used as an outer and inner loop. Using the average model, the eigenvalues of the closed-loop system are investigated. To make the controlled performance independent of the operating point, the eigenvalues of the system must be fixed. It can be performed by using the controller whose designing process does not depend on the operating point of the converter.

The current controller is suitable for some applications, such as the photovoltaic system, where the operating point usually changes. In this paper, these controllers are applied to a boost converter.

The results for the movement of eigenvalues corresponding to the controller design are presented for two cases.

The system can be unstable when the dynamics of the two control loops do not decouple well. The operating point plays a role in this case. The dynamical behavior of the system is subject to temporal fluctuations, originating from variations in load power or modifications in the properties of parasitic elements, resulting in deviations from their nominal values. These alterations in stability characteristics bear implications for the pragmatic application of the boost converter. A thorough investigation into its stability is imperative to delineate a secure operational domain for dependable utilization.

A drawback of this investigation is that achieving a rapid response in the outer loop necessitates acceleration of the inner loop, leading to an eventual requirement for a higher switching frequency.

MATLAB/Simulink software was employed to conduct local stability analysis, showcasing the trajectory of eigenvalues associated with the controller design. This analysis is imperative in the design phase to guarantee stable system operation. The outcomes revealed precise adherence to energy regulation and voltage adjustment to the introduced changes.

However, when the system is well decoupled, as the eigenvalue becomes smaller than in the latter case, the response time of the energy loop becomes longer.

The research contribution is to study the local stability of cascaded control based on indirect-sliding mode and energy concepts because of its benefits in performance and design. The closed-loop poles are fixed independently of operating points, thanks to implementing nonlinear controllers based on a large-signal averaged model without resorting to small-signal linearization. The complete separation dynamics of the inner and outer loops are investigated.

Future endeavors involve the integration of an LC filter at the converter's input to mitigate ripple in the input current. Additionally, there is a plan to explore the system's stability when repositioning the poles of the inner loop to higher levels, catering to the requirements of a constant power load (CPL).

ACKNOWLEDGMENT

This work was supported in part by an International Research Partnership “Electrical Engineering – Thai French Research Center (EE-TFRC)” under the project framework of the Lorraine Université d'Excellence (LUE) in cooperation between Université de Lorraine and King Mongkut's University of Technology North Bangkok and in part by Shahid Beheshti G.C. University.

REFERENCES

[1] T. A. Pereira, L. Schmitz, W. M. dos Santos, D. C. Martins, and R. F. Coelho, "Design of a Portable Photovoltaic I–V Curve Tracer Based on the DC–DC Converter Method," *IEEE J. Photovolt.*, vol. 11, no. 2, pp. 552-560, March 2021, DOI: 10.1109/JPHOTOV.2021.3049903.

[2] Y. Zhuang, F. Liu, X. Zhang, Y. Huang, X. Zha, and Z. Liu, "Short-Circuit Fault-Tolerant Topology for Multiport Cascaded DC/DC Converter in Photovoltaic Power Generation System," *IEEE Trans. Power Electron.*, vol. 36, no. 1, pp. 549-561, Jan. 2021, DOI: 10.1109/TPEL.2020.3004070

[3] S. W. Azeem, W. Chen, I. Tariq, H. Ye, and D. Kaija, "A Hybrid Resonant ZVZCS Three-Level Converter Suitable for Photovoltaic Power DC Distribution System," *IEEE Access*, vol. 8, pp. 114981-114990, 2020, DOI: 10.1109/ACCESS.2020.3002338.

[4] J. W. Zapata, S. Kouro, G. Carrasco, H. Renaudineau, and T. A. Meynard, "Analysis of Partial Power DC–DC Converters for Two-Stage Photovoltaic Systems," *IEEE J. Emerg. Sel. Top. Power Electron.*, vol. 7, no. 1, pp. 591-603, March 2019, DOI: 10.1109/JESTPE.2018.2842638.

[5] G. G. Kumar, K. Sundaramoorthy, V. Karthikeyan, and E. Babaei, "Switched Capacitor–Inductor Network Based Ultra-Gain DC–DC Converter Using Single Switch," *IEEE Trans. Ind. Electron.*, vol. 67, no. 12, pp. 10274-10283, Dec. 2020, DOI: 10.1109/TIE.2019.2962406.

[6] P. K. Pardhi and S. K. Sharma, "High Gain Non Isolated DC Converter Employed in Single-Phase Grid-Tied Solar Photovoltaic Supply System," *IEEE Trans. Ind. Appl.*, vol. 57, no. 5, pp. 5170-5182, Sept.-Oct. 2021, DOI: 10.1109/TIA.2021.3095439.

[7] S. Khan, M. Zaid, M. M. A. Khan, and A. Sarwar, "A Non-Pulsating Input Current Step-Up DC/DC Converter With Common Ground Structure for Photovoltaic Applications," *IEEE Access*, vol. 9, pp. 159432-159446, 2021, DOI: 10.1109/ACCESS.2021.3128255.

[8] P. L. Métayer, Q. Loeuillet, F. Wallart, C. Buttay, D. Dujic, and P. Dworakowski, "Phase-Shifted Full Bridge DC–DC Converter for Photovoltaic MVDC Power Collection Networks," *IEEE Access*, vol. 11, pp. 19039-19048, 2023, DOI: 10.1109/ACCESS.2023.3247952.

[9] R. Rahimi, S. Habibi, P. Shamsi, and M. Ferdowsi, "A Three-Winding Coupled-Inductor-Based Dual-Switch High Step-Up DC–DC Converter for Photovoltaic Systems," *IEEE Journal of Emerging and Selected Topics in Industrial Electronics*, vol. 3, no. 4, pp. 1106-1117, Oct. 2022, DOI: 10.1109/JESTIE.2022.3151554.

[10] R. Rahimi, S. Habibi, M. Ferdowsi, and P. Shamsi, "Z-Source-Based High Step-Up DC–DC Converters for Photovoltaic Applications," *IEEE J. Emerg. Sel. Top. Power Electron.*, vol. 10, no. 4, pp. 4783-4796, Aug. 2022, DOI: 10.1109/JESTPE.2021.3131996.

[11] D. López del Moral, A. Barrado, M. Sanz, A. Lázaro, and P. Zumel, "Analysis, Design, and Implementation of the AFZ Converter Applied to Photovoltaic Systems," *IEEE Trans. Power Electron.*, vol. 36, no. 2, pp. 1883-1900, Feb. 2021, DOI: 10.1109/TPEL.2020.3010152.

[12] R. Rahimi, S. Habibi, M. Ferdowsi, and P. Shamsi, "A Three-Winding Coupled Inductor-Based Interleaved High-Voltage Gain DC–DC Converter for Photovoltaic Systems," *IEEE Trans. Power Electron.*, vol. 37, no. 1, pp. 990-1002, Jan. 2022, DOI: 10.1109/TPEL.2021.3099486.

[13] S. R. Kukunuru, Y. Naeimi, and L. G. Salem, "A Series-Parallel Switched-Photovoltaic DC–DC Converter," *IEEE J. Solid-State Circuits*, vol. 58, no. 3, pp. 742-756, March 2023, DOI: 10.1109/JSSC.2022.3223890.

[14] Y. Zhuang *et al.*, "A Multiport Modular DC–DC Converter With Low-Loss Series LC Power Balancing Unit for MVDC Interface of Distributed Photovoltaics," *IEEE Trans. Power Electron.*, vol. 36, no. 7, pp. 7736-7749, July 2021, DOI: 10.1109/TPEL.2020.3041875.

[15] V. K. Goyal and A. Shukla, "Isolated DC–DC Boost Converter for Wide Input Voltage Range and Wide Load Range Applications," *IEEE Trans. Ind. Electron.*, vol. 68, no. 10, pp. 9527-9539, Oct. 2021, DOI: 10.1109/TIE.2020.3029479.

[16] A. Sarikhani, B. Allahverdinejad, and M. Hamzeh, "A Nonisolated Buck–Boost DC–DC Converter With Continuous Input Current for Photovoltaic Applications," *IEEE J. Emerg. Sel. Top. Power Electron.*, vol. 9, no. 1, pp. 804-811, Feb. 2021, DOI: 10.1109/JESTPE.2020.2985844.

[17] I. A. Reyes-Portillo, J. Morales-Saldaña, C. Romero-Rivera, and E. Palacios-Hernández, "Design and Modeling of a High Current Ratio Converter for PV Applications," *IEEE Lat. Am. Trans.*, vol. 21, no. 10, pp. 1144-1155, Oct. 2023, DOI: 10.1109/TLA.2023.10255452.

[18] Chandrasekar *et al.*, "Non-Isolated High-Gain Triple Port DC–DC Buck-Boost Converter With Positive Output Voltage for Photovoltaic Applications," *IEEE Access*, vol. 8, pp. 113649-113666, 2020, DOI: 10.1109/ACCESS.2020.3003192.

[19] J. Zeng, J. Ning, X. Du, T. Kim, Z. Yang, and V. Winstead, "A Four-Port DC–DC Converter for a Standalone Wind and Solar Energy System," *IEEE Trans. Ind. Appl.*, vol. 56, no. 1, pp. 446-454, 2020, DOI: 10.1109/TIA.2019.2948125.

[20] J. Wang, K. Sun, C. Xue, T. Liu, and Y. Li, "Multi-Port DC-AC Converter With Differential Power Processing DC-DC Converter and Flexible Power Control for Battery ESS Integrated PV Systems," *IEEE Trans. Ind. Electron.*, vol. 69, no. 5, pp. 4879-4889, May 2022, DOI: 10.1109/TIE.2021.3080198.

[21] R. Liu, G. Zhou, Q. Tian, and G. Xu, "Extendable Multiport High Step-Up DC–DC Converter for Photovoltaic-Battery Systems With Reduced Voltage Stress on Switches/Diodes," *IEEE Trans. Ind. Electron.*, vol. 70, no. 9, pp. 9123-9135, Sept. 2023, DOI: 10.1109/TIE.2022.3206752.

[22] J. Zeng, X. Du, and Z. Yang, "A Multiport Bidirectional DC–DC Converter for Hybrid Renewable Energy System Integration," *IEEE Trans. Power Electron.*, vol. 36, no. 11, pp. 12281-12291, Nov. 2021, DOI: 10.1109/TPEL.2021.3082427.

[23] Q. Tian, G. Zhou, M. Leng, G. Xu, and X. Fan, "A Nonisolated Symmetric Bipolar Output Four-Port Converter Interfacing PV-Battery System," *IEEE Trans. Power Electron.*, vol. 35, no. 11, pp. 11731-11744, Nov. 2020, DOI: 10.1109/TPEL.2020.2983113.

[24] M. I. Marei, B. N. Alajmi, I. Abdelsalam, and N. A. Ahmed, "An Integrated Topology of Three-Port DC-DC Converter for PV-Battery Power Systems," *IEEE open j. Ind. Electron.*, vol. 3, pp. 409-419, 2022, DOI: 10.1109/OJIES.2022.3182977.

[25] T. Qian, Y. Yang, and W. Zhao, "A Boost-Type Three-Port Resonant Forward Converter With Flexible Power Flow Path Optimization for PV Systems," *IEEE Trans. Circuits Syst. II Express Briefs*, vol. 70, no. 1, pp. 161-165, Jan. 2023, DOI: 10.1109/TCSII.2022.3199335.

[26] Y. Sato, M. Uno, and H. Nagata, "Nonisolated Multiport Converters Based on Integration of PWM Converter and Phase-Shift-Switched Capacitor Converter," *IEEE Trans. Power Electron.*, vol. 35, no. 1, pp. 455-470, Jan. 2020, DOI: 10.1109/TPEL.2019.2912550.

[27] P. Prabhakaran and V. Agarwal, "Novel Four-Port DC–DC Converter for Interfacing Solar PV–Fuel Cell Hybrid Sources With Low-Voltage Bipolar DC Microgrids," *IEEE J. Emerg. Sel. Top. Power Electron.*, vol. 8, no. 2, pp. 1330-1340, June 2020, DOI: 10.1109/JESTPE.2018.2885613.

[28] S. Lu, K. Sun, H. Shi, Y. Li, and G. Cao, "Evaluation of high step-up power conversion systems for large-capacity photovoltaic generation integrated into medium voltage DC grids," in *Chinese Journal of Electrical Engineering*, vol. 7, no. 4, pp. 3-14, Dec. 2021, DOI: 10.23919/CJEE.2021.000033.

[29] J. Yang, R. Li, K. Ma, and J. Xu, "A Distributed Multimode Control Strategy for the Cascaded DC–DC Converter Applied to MVAC Grid-Tied PV System," *IEEE Trans. Ind. Electron.*, vol. 70, no. 3, pp. 2617-2627, March 2023, DOI: 10.1109/TIE.2022.3174300.

[30] A. A. Hussein, X. Chen, M. Alharbi, A. A. Pise, and I. Batarseh, "Design of a Grid-Tie Photovoltaic System With a Controlled Total Harmonic Distortion and Tri Maximum Power Point Tracking," *IEEE Trans. Power Electron.*, vol. 35, no. 5, pp. 4780-4790, May 2020, DOI: 10.1109/TPEL.2019.2946586.

[31] M. K. Ram, M. N. Anwar, P. Verma, and A. Iqbal, "Closed-Loop Test Based Parametric Independent Control of DC–DC Boost-Converter Using Two Degree of Freedom Internal Model Control Scheme," *IEEE Access*, vol. 11, pp. 76619-76628, 2023, DOI: 10.1109/ACCESS.2023.3297491.

[32] D. R. Espinoza Trejo, S. Taheri, J. L. Saavedra, P. Vázquez, C. H. De Angelo, and J. A. Pecina-Sánchez, "Nonlinear Control and Internal Stability Analysis of Series-Connected Boost DC/DC Converters in PV Systems With Distributed MPPT," *IEEE J. Photovolt.*, vol. 11, no. 2, pp. 504-512, March 2021, DOI: 10.1109/JPHOTOV.2020.3041237.

[33] W. N. D. Silva, L. D. S. Bezerra, S. C. S. Jucá, R. I. S. Pereira, and C. M. d. S. Medeiros, "Control and monitoring of a Flyback DC-DC converter for photovoltaic applications using embedded IoT system," *IEEE Lat. Am. Trans.*, vol. 18, no. 11, pp. 1892-1899, 2020, DOI: 10.1109/TLA.2020.9398630.

[34] Y. Liang, H. Zhang, M. Du, and K. Sun, "Parallel coordination control of multi-port DC-DC converter for stand-alone photovoltaic-energy storage systems," *CPSS trans. power electron. appl.*, vol. 5, no. 3, pp. 235-241, Sept. 2020, DOI: 10.24295/CPSSTPEA.2020.00020.

[35] E. O. B. Luna, C. B. Jacobina, and A. C. Oliveira, "Internal Energy Balance of a Modular Multilevel Cascade Converter Based on Chopper-Cells With Distributed Energy Resources for Grid-Connected Photovoltaic Systems," *IEEE Trans. Ind. Appl.*, vol. 59, no. 2, pp. 1935-1943, March-April 2023, DOI:10.1109/ECCE44975.2020.9236323.

[36] O. Abdel-Rahim and H. Wang, "A new high gain DC-DC converter with model-predictive-control based MPPT technique for photovoltaic

systems," *CPSS trans. power electron. appl.*, vol. 5, no. 2, pp. 191-200, June 2020, DOI: 10.24295/CPSSTPEA.2020.00016.

[37] D. Vinnikov, A. Chub, R. Kosenko, V. Sidorov, and A. Lindvest, "Implementation of Global Maximum Power Point Tracking in Photovoltaic Microconverters: A Survey of Challenges and Opportunities," *IEEE J. Emerg. Sel. Top. Power Electron.*, vol. 11, no. 2, pp. 2259-2280, April 2023, DOI: 10.1109/JESTPE.2021.3137521.

[38] K. Ishaque and Z. Salam, "A Deterministic Particle Swarm Optimization Maximum Power Point Tracker for Photovoltaic System Under Partial Shading Condition," *IEEE Trans. Ind. Electron.*, vol. 60, no. 8, pp. 3195-3206, 2012, DOI: 10.1109/TIE.2012.2200223.

[39] M. Azmi, S. M. Noor, and S. Musa, "Fuzzy logic control based maximum power point tracking technique in stand alone photovoltaic system," *Int. J. Power Electron. Drive Syst.*, vol. 14, No. 2, pp. 1110-1120, June 2023, DOI: https://doi.org/10.1007/978-981-19-4975-3_11.

[40] T. Sutikno, A. C. Subrata, and A. Elkhateb, "Evaluation of Fuzzy Membership Function Effects for Maximum Power Point Tracking Technique of Photovoltaic System," *IEEE Access*, vol. 9, pp. 109157-109165, 2021, DOI: 10.1109/ACCESS.2021.3102050.

[41] M. -C. Chang and S. -I. Liu, "An Indoor Photovoltaic Energy Harvester Using Time-Based MPPT and On-Chip Photovoltaic Cell," *IEEE Trans. Circuits Syst. II Express Briefs*, vol. 67, no. 11, pp. 2432-2436, Nov. 2020, DOI: 10.1109/TCSII.2020.2976760.

[42] C. Rao, A. Hajjiah, M. A. El-Meligy, M. Sharaf, A. T. Soliman, and M. A. Mohamed, "A Novel High-Gain Soft-Switching DC-DC Converter With Improved P&O MPPT for Photovoltaic Applications," *IEEE Access*, vol. 9, pp. 58790-58806, 2021, DOI: 10.1109/ACCESS.2021.3072972.

[43] J. -E. Hernández-Díez, C. -F. Méndez-Barrios, S. -I. Niculescu, and E. Bárcenas-Bárcenas, "A Current Sensorless Delay–Based Control Scheme for MPPT–Boost Converters in Photovoltaic Systems," *IEEE Access*, vol. 8, pp. 174449-174462, 2020, DOI: 10.1109/ACCESS.2020.3024566.

[44] R. Kahani, M. Jamil, and M. T. Iqbal, "An Improved Perturb and Observed Maximum Power Point Tracking Algorithm for Photovoltaic Power Systems," *J. Mod. Power Syst. Clean Energy*, vol. 11, no. 4, pp. 1165-1175, July 2023, DOI: 10.35833/MPCE.2022.000245.

[45] A. Hafian, M. Benbrahim, and M. N. Kabba, "A novel algorithm for optimal sizing of stand-alone photovoltaic pumping systems," *Int. J. Power Electron. Drive Syst.*, vol. 13, No. 3, pp. 1833-1842, 2022, DOI: 10.11591/ijpeds.v13.i3.

[46] M. Bahrami *et al*., "Hybrid maximum power point tracking algorithm with improved dynamic performance," *Renew. Energ.*, vol. 130, pp. 982-991, 2019, DOI: 10.1016/j.renene.2018.07.020.

[47] H. Oufettoul, N. Lamdihine, S. Motahhir, N. Lamrini, I. A. Abdelmoula, and G. Aniba, "Comparative Performance Analysis of PV Module Positions in a Solar PV Array Under Partial Shading Conditions," *IEEE Access*, vol. 11, pp. 12176-12194, 2023, doi: 10.1109/ACCESS.2023.3237250.

[48] R. K. Pachauri, I. Kansal, T. S. Babu, and H. H. Alhelou, "Power Losses Reduction of Solar PV Systems Under Partial Shading Conditions Using Re-Allocation of PV Module-Fixed Electrical Connections," *IEEE Access*, vol. 9, pp. 94789-94812, 2021, DOI: 10.1109/ACCESS.2021.3093954.

[49] K. Abdulmawjood, S. Alsadi, S. S. Refaat, and W. G. Morsi, "Characteristic Study of Solar Photovoltaic Array Under Different Partial Shading Conditions," *IEEE Access*, vol. 10, pp. 6856-6866, 2022, DOI: 10.1109/ACCESS.2022.3142168.

[50] C. Saiprakash, A. Mohapatra, B. Nayak, T. S. Babu, and H. H. Alhelou, "A Novel Benzene Structured Array Configuration for Harnessing Maximum Power From PV Array Under Partial Shading Condition With Reduced Number of Cross Ties," *IEEE Access*, vol. 10, pp. 129712-129726, 2022, DOI: 10.1109/ACCESS.2022.3228049.

[51] S. Bouguerra, M. R. Yaiche, O. Gassab, A. Sangwongwanich, and F. Blaabjerg, "The Impact of PV Panel Positioning and Degradation on the PV Inverter Lifetime and Reliability," *IEEE J. Emerg. Sel. Top. Power Electron.*, vol. 9, no. 3, pp. 3114-3126, June 2021, DOI: 10.1109/JESTPE.2020.3006267.

[52] V. Poulek *et al.*, "PV Panel and PV Inverter Damages Caused by Combination of Edge Delamination, Water Penetration, and High String Voltage in Moderate Climate," *IEEE J. Photovolt.*, vol. 11, no. 2, pp. 561-565, March 2021, DOI: 10.1109/JPHOTOV.2021.3050984.

[53] T. Tafticht, Mr Tchakala, and M. J. Rahman, "GMPPT approach for photovoltaic systems under partial shading conditions using a genetic algorithm," *Int. J. Power Electron. Drive Syst.*, vol. 13, No. 2, pp. 1238-1245, June 2022, DOI:10.11591/ijpeds.v13.i2.

[54] M. G. Yahya and M. G. Yahya, "Modified PDPWM control with MPPT algorithm for equal power sharing in cascaded multilevel inverter for stand alone PV system under partial shading," *Int. J. Power Electron. Drive Syst.*, vol. 14, No. 1, pp. 533-545, March 2023, DOI: 10.11591/ijpeds.v14.i1.pp533-545.

[55] V. S. Bhadoria, R. K. Pachauri, S. Tiwari, S. P. Jaiswal, and H. H. Alhelou, "Investigation of Different BPD Placement Topologies for Shaded Modules in a Series-Parallel Configured PV Array," *IEEE Access*, vol. 8, pp. 216911-216921, 2020, DOI: 10.1109/ACCESS.2020.3041715.

[56] Z. Alqaisi and Y. Mahmoud, "Comprehensive Study of Partially Shaded PV Modules With Overlapping Diodes," *IEEE Access*, vol. 7, pp. 172665-172675, 2019, DOI: 10.1109/ACCESS.2019.2956916.

[57] F. Alonge, F. D'ippolito, G. Garraffa, G. C. Giaconia, R. Latona, and A. Sferlazza, "Sliding Mode Control of Quadratic Boost Converters Based on Min-Type Control Strategy," *IEEE Access*, vol. 11, pp. 39176-39184, 2023, DOI: 10.1109/ACCESS.2023.3267984.

[58] L. M. Saublet, R. Gavagsaz-Ghoachani, J. P. Martin, B. Nahid-Mobarakeh, and S. Pierfederici, "Bifurcation analysis and stabilization of DC power systems for electrified transportation systems," *IEEE Trans. Transp. Electrific.*, vol. 2, no. 1, pp. 86–95, Mar. 2016, DOI: 10.1109/TTE.2016.2519351.

[59] A. Battiston, E. -H. Miliani, J. -P. Martin, B. Nahid-Mobarakeh, S. Pierfederici, and F. Meibody-Tabar, "A Control Strategy for Electric Traction Systems Using a PM-Motor Fed by a Bidirectional Z -Source Inverter," *IEEE Trans. Veh. Technol.*, vol. 63, no. 9, pp. 4178-4191, Nov. 2014, DOI: 10.1109/TVT.2014.2312434.

[60] R. Gavagsaz-Ghoachani, M. Phattanasak, J. -P. Martin, B. Nahid-Mobarakeh, and S. Pierfederici, "A Fixed-Frequency Optimization of PWM Current Controller—Modeling and Design of Control Parameters," *IEEE Trans. Transp. Electrific.*, vol. 4, no. 3, pp. 671-683, Sept. 2018, DOI: 10.1109/TTE.2018.2841801.

[61] M. Afkar, R. Gavagsaz-Ghoachani, M. Phattanasak, and S. Pierfederici, "Cascaded Controller for Controlling DC Bus Voltage in Mismatched Input Powers," *IEEE Trans. Power Electron.*, vol. 37, no. 11, pp. 13834-13847, Nov. 2022, DOI: 10.1109/TPEL.2022.3186233.

[62] A. Shahin *et al.*, "Sensorless Robust Flatness-Based Control With Nonlinear Observer for Non-Ideal Parallel DC–AC Inverters," *IEEE Access*, vol. 10, pp. 53940-53953, 2022, DOI: 10.1109/ACCESS.2022.3175847.

[63] D. Dell'Isola, M. Urbain, M. Weber, S. Pierfederici, and F. Meibody-Tabar, "Optimal Design of a DC–DC Boost Converter in Load Transient Conditions, Including Control Strategy and Stability Constraint," *IEEE Trans. Transp. Electrification.*, vol. 5, no. 4, pp. 1214-1224, Dec. 2019, DOI: 10.1109/TTE.2019.2948038.

[64] R. Choupanzadeh and A. Zadehgol, "Stability, Causality, and Passivity of Canonical Equivalent Circuits for Improper Rational Transfer Functions—Part II: With Complex-Conjugate Poles and Residues," *IEEE Access*, vol. 11, pp. 108995-109009, 2023, DOI: 10.1109/ACCESS.2023.3321631.

[65] Z. Shahrouei, M. Rahmati, R. Gavagsaz-Ghoachani, M. Phattanasak, J. -P. Martin, and S. Pierfederici, "Robust Flatness-Based Control With Nonlinear Observer for Boost Converters," *IEEE Trans. Transp. Electrification.*, vol. 9, no. 1, pp. 142-155, March 2023, DOI: 10.1109/TTE.2022.3192217.

[66] Y. Hennane, S. Pierfederici, A. Berdai, F. Meibody-Tabar, and J. -P. Martin, "Distributed Control of Islanded Meshed Microgrids," *IEEE Access*, vol. 11, pp. 78262-78272, 2023, DOI: 10.1109/ACCESS.2023.3298525.

[67] M. Afkar, R. Gavagsaz-Ghoachani, M. Phattanasak, J. -P. Martin, and S. Pierfederici, "Proposed System Based on a Three-Level Boost Converter to Mitigate Voltage Imbalance in Photovoltaic Power Generation Systems," *IEEE Trans. Power Electron.*, vol. 37, no. 2, pp. 2264-2282, Feb. 2022, DOI: 10.1109/TPEL.2021.3105571.

[68] P. Thounthong *et al.*, "Robust Hamiltonian Energy Control Based on Lyapunov Function for Four-Phase Parallel Fuel Cell Boost Converter for DC Microgrid Applications," *IEEE Trans Sustain Energy.*, vol. 12, no. 3, pp. 1500-1511, July 2021, DOI: 10.1109/TSTE.2021.3050783.

[69] P. Mungporn *et al.*, "Modeling and Control of Multiphase Interleaved Fuel-Cell Boost Converter Based on Hamiltonian Control Theory for Transportation Applications," *IEEE Trans. Transp. Electrification.*, vol. 6, no. 2, pp. 519-529, June 2020, DOI: 10.1109/TTE.2020.2980193.

[70] S. Pang *et al.*, "Large-Signal Stabilization of Power Converters Cascaded Input Filter Using Adaptive Energy Shaping Control," *IEEE Trans. Transp. Electrification.*, vol. 7, no. 2, pp. 838-853, June 2021, DOI: 10.1109/TTE.2020.3021954.

[71] B. Yodwong, S. Sikkabut, D. Guilbert, M. Hinaje, P. Phattanasak, W. Kaewmanee, and G. Vitale, "Open-Circuit Switch Fault Diagnosis and Accommodation of a Three-Level Interleaved Buck Converter for Electrolyzer Applications," *Electronics*, vol. 12, pp. 1-24, 2023, DOI: 10.3390/electronics12061349.

[72] B. Yodwong, D. Guilbert, W. Kaewmanee, M. Phattanasak, M. Hinaje, and G. Vitale, "Improved Sliding Mode-Based Controller of a High Voltage Ratio DC–DC Converter for Electrolyzers Supplied by Renewable Energy," *IEEE Trans. Ind. Electron.*, DOI: 10.1109/TIE.2023.3322009.

[73] M. Afkar, R. Gavagsaz-Ghoachani, M. Phattanasak, A. Siangsanoh, J. -P. Martin, and S. Pierfederici, "Generalization of a DC–DC Modular Converter Topology for Fuel Cell Applications," *IEEE Trans. Ind. Appl.*, vol. 58, no. 2, pp. 2255-2267, 2022, DOI: 10.1109/TIA.2022.3142659.

[74] Z. Liu *et al.*, "Existence and Stability of Equilibrium of DC Micro-Grid Under Master-Slave Control," *IEEE Trans. Power Syst.*, vol. 37, no. 1, pp. 212-223, Jan. 2022, DOI: 10.1109/TPWRS.2021.3085872.

[75] Y. L. Guo, L. Wang, and Q. H. Wu, "Bifurcation Control Method for Buck-Boost Converters Based on Energy Balance Principle," *IEEE J. Emerg. Sel. Top. Power Electron.*, vol. 9, no. 6, pp. 6947-6954, Dec. 2021, DOI: 10.1109/JESTPE.2021.3067357.

[76] P. Azer and A. Emadi, "Generalized State Space Average Model for Multi-Phase Interleaved Buck, Boost and Buck-Boost DC-DC Converters: Transient, Steady-State and Switching Dynamics," *IEEE Access*, vol. 8, pp. 77735-77745, 2020, DOI: 10.1109/ACCESS.2020.2987277.

[77] M. Bahrami, J. -P. Martin, G. Maranzana, S. Pierfederici, F. Meibody-Tabar, and M. Weber, "Hybrid power electronics architecture to implement the fuel cell management system," *2020 IEEE Energy Conversion Congress and Exposition (ECCE)*, 2020, DOI: 10.1109/ECCE44975.2020.9235418.

[78] M. Amin and M. Molinas, "Small-Signal Stability Assessment of Power Electronics Based Power Systems: A Discussion of Impedance- and Eigenvalue-Based Methods," *IEEE Trans. Ind. Appl.*, vol. 53, no. 5, pp. 5014-5030, 2017, DOI: 10.1109/TIA.2017.2712692.

[79] K. Ogata. *Modern Control Engineering 5th Edition*. Pearson, 2010.

[80] J. D. Navamani, K. Boopathi, M. J. Sathik, A. Lavanya, Kitmo, and P. Vishnuram, "Analysis of Higher Dimensional Converter Using Graphical Approach," *IEEE Access*, vol. 11, pp. 75076-75092, 2023, DOI: 10.1109/ACCESS.2023.3295996.